inorganics

MDPI

Article

Toward Photoactivatable Copper(I) Anticancer Agents: Heteroleptic Cu(I) Complexes with Functionalized Dipyridylamine Ligands

Alondra Villegas-Menares [1,2,*], María Herrera-Maldonado [3], Iván Brito [4], Michelle Palacios [1], Sebastián Muñoz-Farias [3], Mario A. Faundez [5] and Alan R. Cabrera [1,*]

[1] Departamento de Química Inorgánica, Escuela de Química, Facultad de Química y de Farmacia, Pontificia Universidad Católica de Chile, Vicuña Mackenna 4860, Macul, Santiago 7820436, Chile
[2] Escuela de Obstetricia y Puericultura y Centro de Estudios e Investigación en Salud y Sociedad (CEISS), Facultad de Ciencias Médicas, Universidad Bernardo O'Higgins, General Gana 1702, Santiago 8370993, Chile
[3] Departamento de Química, Facultad de Ciencias Naturales, Matemática y del Medio Ambiente, Universidad Tecnológica Metropolitana, Las Palmeras 3360, Ñuñoa, Santiago 7800003, Chile
[4] Departamento de Química, Facultad de Ciencias Básicas, Universidad de Antofagasta, Av. Angamos 601, Antofagasta 1270300, Chile
[5] Departamento de Farmacia, Escuela de Química y Farmacia, Facultad de Química y de Farmacia, Pontificia Universidad Católica de Chile, Vicuña Mackenna 4860, Macul, Santiago 7820436, Chile
* Correspondence: alondra.villegas@ubo.cl (A.V.-M.); arcabrer@uc.cl (A.R.C.)

Abstract

In this study, we report the synthesis and characterization of three Cu(I) complexes bearing functionalized dipyridylamine ligands and DPEphos. Structural analysis confirms a distorted tetrahedral coordination environment around the metal center. Photophysical studies in DMSO show similar absorption profiles ($\lambda_{abs} \approx 341$–$343$ nm) with ligand-centered and MLCT transitions, while emission spans the visible region ($\lambda_{emi} = 410$–483 nm) and is strongly influenced by ligand substitution, with the CF_3 derivative displaying a marked red shift. Emission is insensitive to oxygen and exhibits short lifetimes ($\tau \approx 14.9$–15.3 ns), suggesting short-lived ^{1}MLCT excited states. Biological evaluation in A375 melanoma cells reveals that all complexes exhibit low-micromolar cytotoxicity under dark conditions ($IC_{50} = 3.33$–4.92 μM). Notably, only the CF_3-substituted complex shows a significant light-induced enhancement of activity upon irradiation at 390 nm ($IC_{50} = 1.18$ μM), indicating photoactivation.

Keywords: copper (I); dipyridylamine; antitumoral activity; PDT

Check for updates

Academic Editors: Ana Maria Da Costa Ferreira and João Honorato de Araujo-Neto

Received: 9 April 2026
Revised: 6 May 2026
Accepted: 12 May 2026
Published: 19 May 2026

Copyright: © 2026 by the authors. Licensee MDPI, Basel, Switzerland. This article is an open access article distributed under the terms and conditions of the Creative Commons Attribution (CC BY) license.

1. Introduction

Copper(I) complexes have emerged as promising alternatives to noble metal-based systems in both medicinal and photochemical applications, thanks to their earth-abundant, low-cost nature and versatile photophysical properties [1,2]. In particular, heteroleptic Cu(I) complexes with diimine and phosphine ligands have attracted significant attention due to their tunable electronic structures, strong metal-to-ligand charge-transfer (MLCT) transitions, and ability to access long-lived excited states [3–6]. These features have rendered Cu(I) complexes attractive for a variety of applications, from light-emitting devices and photocatalysis to, more recently, bioinorganic and medicinal chemistry [7,8].

Among the various ligand platforms available, dipyridylamine (dpa) derivatives stand out as a particularly attractive class due to their modularity and ability to precisely

adjust both steric and electronic environments around the metal center [1,9–12]. Systematic substitution on the dpa scaffold enables rational control over coordination geometry, redox potentials, and photophysical properties, which are key parameters for designing functional Cu(I) systems [10,11,13]. When combined with appropriate auxiliary ligands, these heteroleptic architectures can stabilize the Cu(I) center while modulating excited-state properties relevant to biological applications [14].

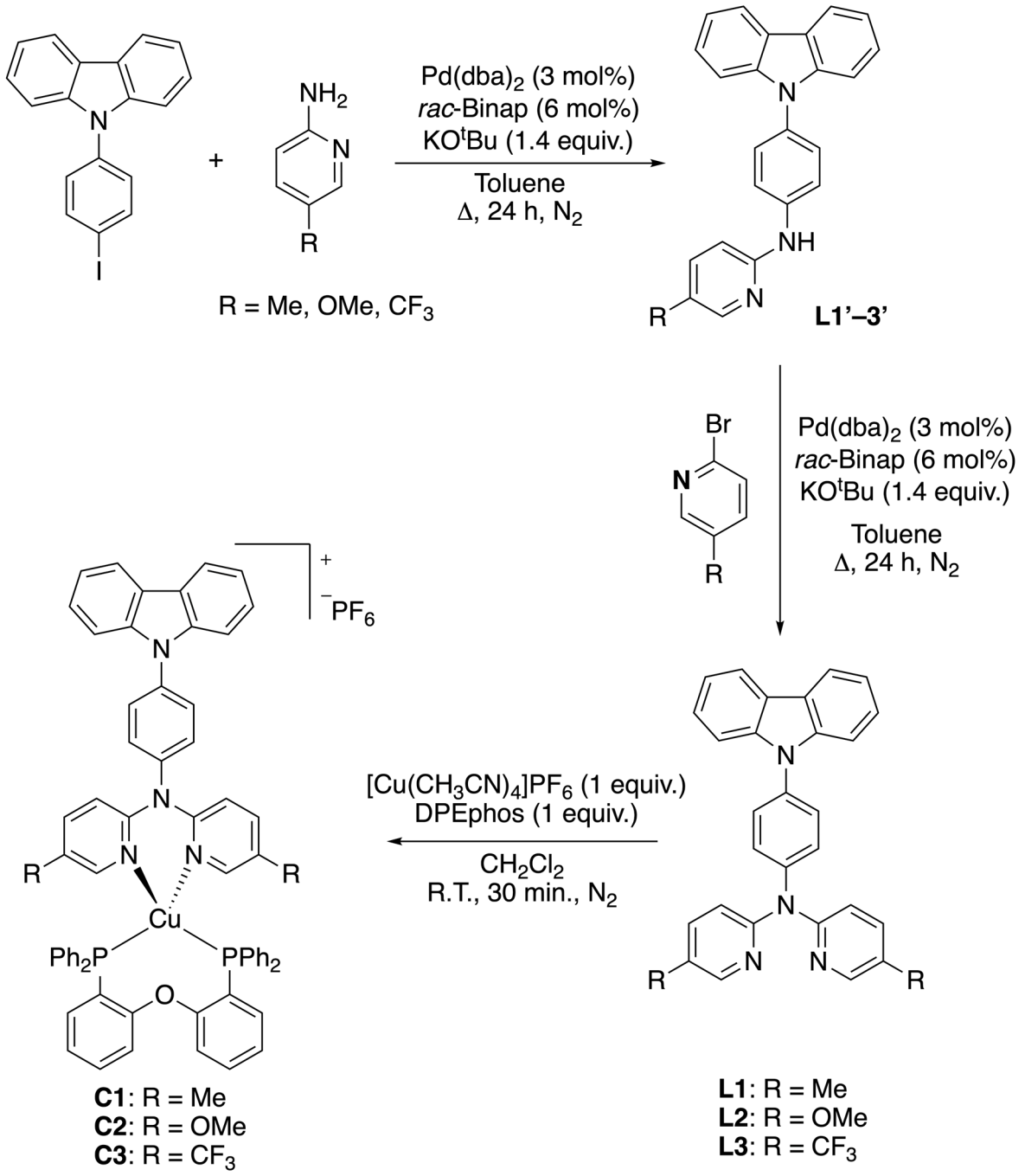
In recent years, increasing attention has been directed toward the development of metal-based compounds with antitumoral activity [15]. In this context, copper complexes have attracted considerable interest due to their rich coordination chemistry and highly tunable structural and electronic properties. These systems have exhibited cytotoxic effects against a variety of cancer cell lines, often mediated by diverse mechanisms of action, including reactive oxygen species (ROS) generation, DNA interactions, and mitochondrial dysfunction [15–19]. Importantly, incorporating photoactive features into such systems opens new avenues for photodynamic therapy (PDT) and, more recently, in photoactivated chemotherapy (PACT), enabling spatial and temporal control of cytotoxicity via light activation [20–25]. To date, however, reports of Cu(I) complexes exhibiting robust photocytotoxic activity remain extremely scarce, with only a single well-documented example, a homoleptic Cu(I) diimine complex, reported in the literature [21]. This limited precedent underscores the challenges associated with simultaneously achieving efficient photoactivity and biological stability in Cu(I)-based systems.

In this context, heteroleptic Cu(I) complexes incorporating dpa-derived ligands represent a compelling platform for developing dual-function agents that combine intrinsic cytotoxicity with potential photoinduced antitumoral activity. The presence of MLCT states that can sensitize molecular oxygen or generate reactive intermediates upon irradiation makes these systems particularly attractive for light-triggered therapeutic strategies. In this study, we report the design, synthesis, and comprehensive characterization of three heteroleptic Cu(I) complexes bearing functionalized dpa ligands, and evaluate their photophysical properties and cytotoxic activity to explore their potential as photoactive anticancer agents.

2. Results and Discussion

2.1. Synthesis and Characterization of Ligands and Complexes

The synthetic route starts with the preparation of the intermediate ligands (**L1′–3′**), which are secondary amines, as shown in Scheme 1. These compounds are produced via a Buchwald–Hartwig coupling between 9-(4-iodophenyl)-9*H*-carbazole and the corresponding 2-amine pyridine derivative [26]. The crude products were purified through column chromatography on silica gel using petroleum ether/ethyl acetate (30–50%) as the eluent. After isolating the intermediate ligands, the same coupling method is used to synthesize the final ligands (**L1–3**). These were obtained in good yields, ranging from 55% to 88%. Once isolated, these were characterized structurally by NMR, FT-IR, and EA. For **L2** and **L3**, the molecular structures were confirmed by single-crystal X-ray diffraction (XRD), as shown in Figures S14 and S19, respectively. The NMR data for both the intermediate and final ligands are consistent with the proposed structures. In the case of **L1′–3′**, the appearance of the N–H proton at a lower field, compared to the $–NH_2$ precursor, confirms the success of the coupling reaction. Conversely, for **L1–3**, the disappearance of the N–H proton confirms the coupling of the second pyridine fragment into the molecule, along with an increase in the integration of the protons belonging to the symmetric pyridinyl group. For details about the characterization of the compounds, see the Supplementary Materials.



Scheme 1. Synthetic route to the obtention of ligands **L1–3** and complexes **C1–3**.

The heteroleptic copper (I) complexes (**C1–3**) were synthesized through a one-pot reaction, as illustrated in Scheme 1, following previous reports [10]. Here, one equivalent of each solid reactant (Cu(I) precursor, DPEphos, and *N*,*N* ligand) is placed into a glass vial, purged with nitrogen, and then dry dichloromethane is added as the solvent. After 30 min, the mixture is filtered, the volatiles are removed, and the product is obtained by crystallization at −20 °C (see the ESI). The Cu(I) complexes **C1–3** were obtained as yellow powders in excellent yields (93–97%) and were thoroughly characterized by NMR, FT-IR, E.A., and XRD (for **C1**).

In the ^{1}H NMR spectra, all three compounds show the expected dominance of aromatic-region resonances, consistent with the coordinated dpa and phosphine ligands. Complex **C1** displays a characteristic singlet at δ 1.85 ppm (6H) due to methyl substituents,

while **C2** shows a singlet at δ 3.41 ppm (6H) assigned to methoxy groups. Conversely, **C3** lacks aliphatic substituent signals, aligning with the proposed ligand framework. The $^{13}C\{^1H\}$ NMR spectra further support this, showing the expected number of aromatic carbon resonances, along with diagnostic signals for the substituents at δ 17.50 ppm (**C1**) and δ 55.91 ppm (**C2**). In all cases, several carbon resonances appear as triplets owing to C–P coupling, confirming the presence of coordinated phosphorus-containing ligands. The $^{31}P\{^1H\}$ NMR spectra of **C1**–**3** each show two clear resonances: a singlet at ≈δ − 13.3 ppm assigned to the coordinated phosphine, and a heptet at about δ − 144.6 ppm arising from the PF_6^- counterion (J^{P-F} ≈ 713–717 Hz). Similarly, the ^{19}F NMR spectra exhibit a doublet at roughly δ − 74.0 ppm with a large F–P coupling constant (J^{F-P} ≈ 720 Hz), which is also characteristic of hexafluorophosphate.

Suitable single crystals for XRD of **C1** were obtained by slow diffusion of pentane into a dichloromethane solution of the complex at low temperature (−20 °C). The molecular structure was successfully solved (Figure 1) and refined at the anisotropic level. Selected distances and angles are summarized in Tables S1 and S2. The molecular structure confirms the formation of the proposed heteroleptic Cu(I) complex, as inferred from NMR characterization. The geometry around the Cu(I) center can be quantified by the τ_4' parameter [27], which is 0.89 for **C1**, indicating a coordination environment slightly distorted from the ideal tetrahedral geometry (τ_4' = 1), consistent with the hindrance exerted by the dpa and DPEphos ligands. The *N*,*N*-chelating unit forms a six-membered metallacycle that adopts a boat-like conformation rather than a planar one (Cu–N1–C00C–N2 = −24.9(9)°). This deformation arises from coordination to the Cu(I) center, combined with steric interactions imposed by the bulky phosphine ligand, as is commonly observed for this class of complexes [10]. The PF_6^- counterion is present but does not participate in coordination, as expected.

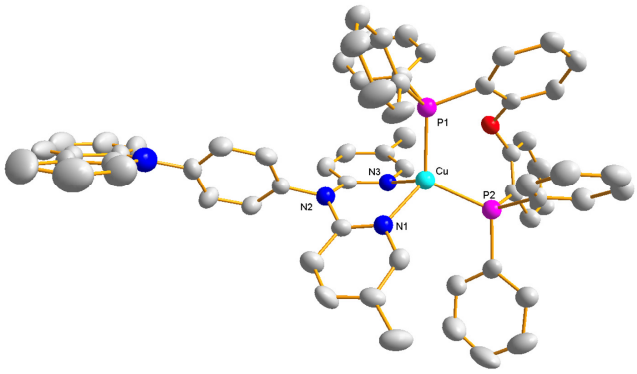


Figure 1. ORTEP plot of complex **C1**, with partial numeration scheme. Hydrogen atoms and the counterion were removed for clarity. Thermal ellipsoids were drawn with 30% of probability.

To evaluate the stability of the complexes under conditions relevant to their handling and biological studies, a time-dependent ^1H and ^{31}P NMR experiment was conducted in DMSO-d_6, using **C1** as a representative example. The spectra were recorded over an extended period (t = 0, 1 day, 3 days, 1 week, and 1 month) under ambient conditions (Figures S40 and S41). Throughout the monitoring period, no significant changes in the spectral profile were observed, and all characteristic resonances remained unchanged in position and intensity. These results indicate that complex **C1** is stable in DMSO solution over time, and similar stability is expected for the related complexes in the series.

2.2. Absorption and Emission Spectroscopic Study of **C1**–**3**

The absorption spectra of complexes **C1**–**3** were recorded in DMSO as the solvent, as depicted in Figure 2, and the data are summarized in Table 1. All complexes display

very similar profiles, with a strong, high-energy absorption band in the UV region (around 290 nm), attributed to ligand-centered (LC) π–π* transitions of the dpa and phosphine ligands [10,28]. This is followed by a broader, less intense shoulder around 350 nm. The position and shape of this lower-energy band show only minor variations among **C1–3**, indicating that the different substituents on the ligands have a limited effect on the frontier molecular orbitals. This band is attributed to metal-to-ligand charge transfer (MLCT) transitions, typical of heteroleptic Cu(I) diimine–DPEphos systems [10,28].

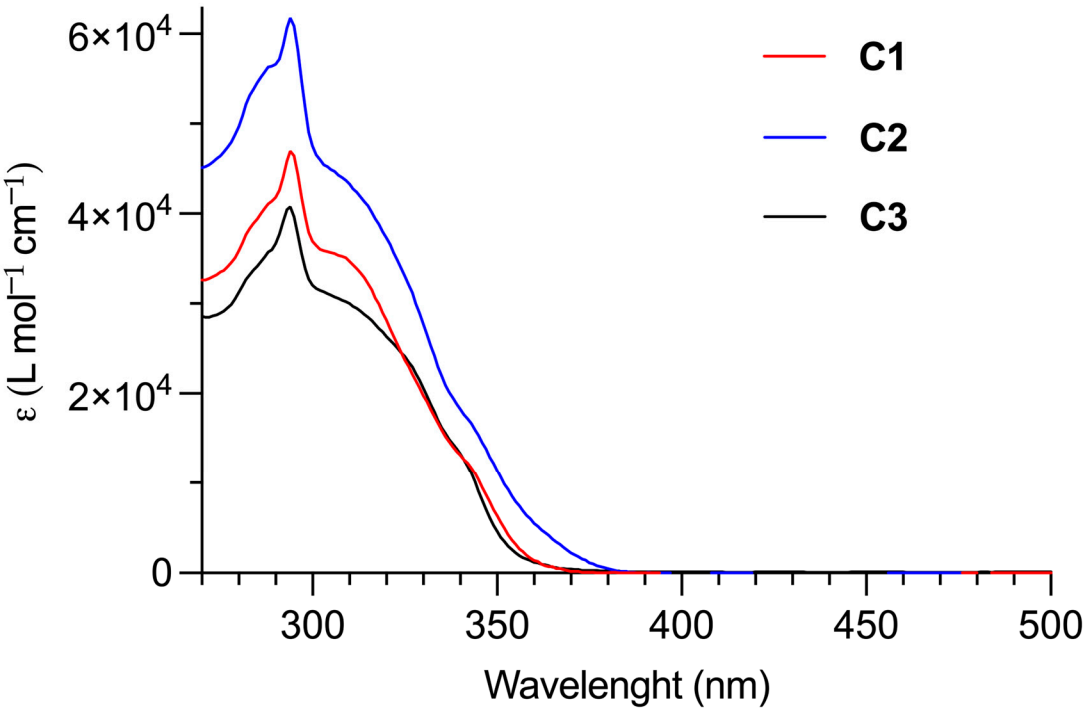


Figure 2. UV-Vis absorption spectra of **C1–3** in DMSO.

Table 1. Summary of absorption and emission data of complexes **C1–3** [a].

Complex	λ_{abs} [nm]	λ_{emi} [nm]	ϕ [b]	τ [ns]
C1	342	410	0.19	14.9
C2	343	427	0.18	15.3
C3	341	483	0.37	15.2

[a] All measurements were recorded in DMSO as the solvent. For the emission data, all values were taken from the deaerated measurements. [b] Estimated using [Cu(dmp)(POP)]BF_4 en CH_2Cl_2 as a standard (fPLQY = 0.15) [29,30].

On the other hand, the emission spectra of complexes **C1–3** were recorded in DMSO under deaerated conditions (Figure 3). The data of this study are summarized in Table 1. The complexes exhibit similar spectral profiles, with broad, structureless emission bands in the visible region between 410 and 483 nm, consistent with predominantly emissive MLCT states typically observed in heteroleptic Cu(I) diimine–phosphine systems [4,10,28]. The electron-donating groups in **C1** (CH_3) and, particularly, **C2** (OCH_3) tend to destabilize the ligand π* orbitals, leading to slightly higher-energy (blue-shifted) emission. In contrast, the strongly electron-withdrawing CF_3 group in **C3** stabilizes the π* orbitals, resulting in a relative red shift in the emission band.

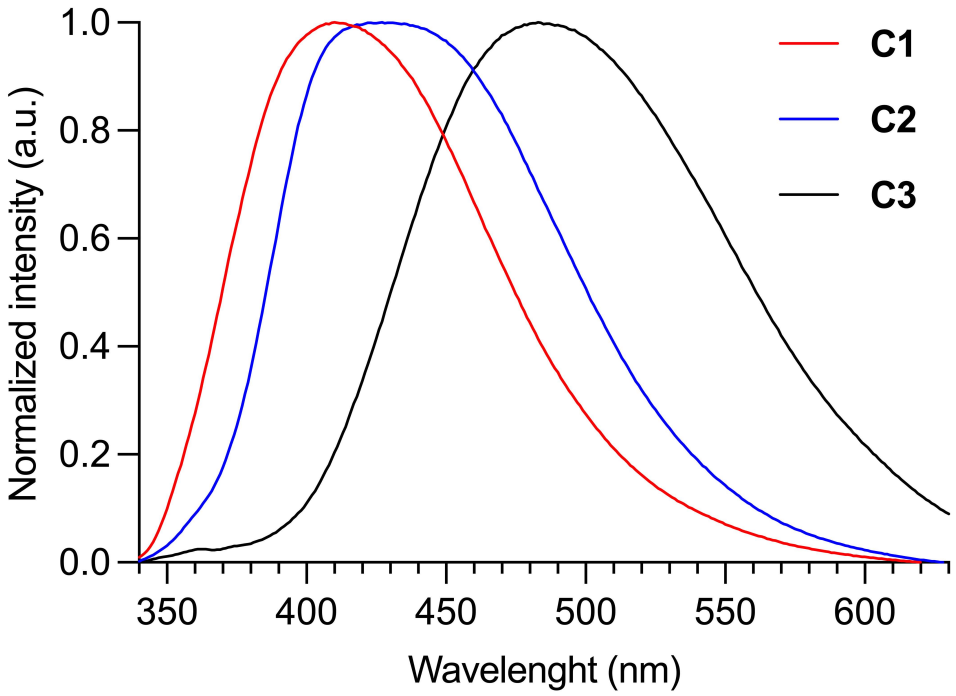


Figure 3. Normalized emission spectra of **C1**–**3** in deoxygenated DMSO.

To determine the nature of the emitter state, the spectra were recorded under air-equilibrated DMSO solutions (Figure S36). Notably, no significant differences in emission intensity or band shape were observed upon removal of dissolved oxygen, suggesting that the excited states are not efficiently quenched by molecular oxygen. This behavior indicates that the emissive state could correspond to a prompt fluorescence of ^{1}MLCT nature [31,32].

2.3. In Vitro Cytotoxicity Assay

The cytotoxic activity of all ligands and complexes was evaluated in A375 melanoma cells under dark conditions and upon irradiation at 390 nm, using the Neutral Red uptake assay. The results are summarized in Table 2, and the dose–response graphs are shown in Figures S43–S46. A clear distinction in biological behavior is observed between the free ligands (**L1**–**3**) and their corresponding Cu(I) complexes (**C1**–**3**). The ligands exhibit no measurable cytotoxicity (IC_{50} > 50 μM) under either condition, confirming that the organic frameworks alone are biologically inactive within the concentration range explored.

Table 2. IC_{50} values for ligands and Cu(I) complexes in A375 cells under dark and light conditions [a].

Entry	Compounds	IC50 [μM] Dark	IC50 [μM] Light [b]
1	**L1**	>50	>50
2	**L2**	>50	>50
3	**L3**	>50	>50
4	**C1**	4.92 ± 0.19	5.20 ± 0.21
5	**C2**	3.33 ± 0.65	4.44 ± 0.39
6	**C3**	4.80 ± 0.66	1.18 ± 0.25
7	Cisplatin	5.50 ± 0.73	5.97 ± 0.17

[a] Values are expressed as mean ± SEM of three independent experiments, each performed in triplicate. [b] LED light 390 nm.

In contrast, all three Cu(I) complexes exhibit significant cytotoxicity in the dark, with IC_{50} values in the low-micromolar range (3.33–4.92 μM), comparable to or exceeding that of cisplatin (5.50 ± 0.73 μM). In this series, all complexes exhibit comparable activity in

the low-micromolar range under dark conditions, with no clear substituent-dependent trend. Importantly, the comparable activity of **C1**–**3** relative to cisplatin indicates that these Cu(I) complexes are promising candidates as chemotherapeutic agents based on earth-abundant metals.

Upon irradiation at 390 nm, distinct behaviors are observed within the complex series. Complexes **C1** and **C2** show no significant improvement in cytotoxicity, with IC_{50} values remaining similar to or slightly higher than under dark conditions. In contrast, **C3** exhibits a pronounced light-induced enhancement of cytotoxicity, with the IC_{50} decreasing from 4.80 ± 0.66 μM in the dark to 1.18 ± 0.25 μM under irradiation, corresponding to an approximately fourfold increase in potency. This result clearly demonstrates that **C3** (CF_3-containing complex) is photoactivatable. In contrast, the modest or negligible differences observed for **C1** and **C2** indicate that their activity is primarily driven by intrinsic cytotoxicity rather than photoactivation.

The photobiological behavior appears to correlate more closely with the nature of the relaxed excited state than with the emission lifetime. In this series, the bathochromic shift in the emission of **C3** may reflect an excited-state electronic structure better suited for photochemical activation, which could account for its significantly enhanced cytotoxicity upon irradiation. However, further studies are required to establish a clear mechanistic relationship between the photophysical properties and the observed photocytotoxic activity.

3. Materials and Methods

3.1. General Information

Tetrakis(acetonitrile)copper(I) hexafluorophosphate, Bis[(2-diphenylphosphino)phenyl] ether (DPEphos), and the pyridine derivatives were purchased from commercial sources and were used without further purification. Solvents (dichloromethane, petroleum ether, ethyl acetate, pentane, and toluene) were obtained from commercial sources and, when necessary, dried with activated molecular sieves. 9-(4-iodophenyl)-9*H*-carbazole was synthesized following the reported literature [33]. NMR spectra were recorded on a Bruker AVANCE 400 instrument (Billerica, MA, USA). Chemical shifts are given in parts per million relative to TMS [^{1}H and ^{13}C, $\delta(SiMe_4) = 0.0$] or an external standard [$\delta(CFCl_3) = 0.0$ for ^{19}F NMR and $\delta(H_3PO_4) = 0.0$ for ^{31}P NMR]. Additional 2D experiments supported most NMR assignments. FT-IR spectra were recorded on a Shimadzu IRTracer-100 Spectrophotometer (Kyoto, Japan), using potassium bromide (KBr) as the solid matrix. Elemental analysis was carried out using an Elementar Analysensysteme GmbH (Langenselbold, Germany), Model Vario EL III. Absorption spectra were recorded using a Shimadzu UV-1900i spectrophotometer (Kyoto, Japan) at room temperature (293 K). Emission spectra were measured using a HORIBA FluoroMax-4 fluorometer (Kyoto, Japan). Time-resolved fluorescence decays were measured in a LifeSpec II fluorescence lifetime spectrometer (Edinburgh Instruments Ltd., Livingston, UK) with a picosecond time resolution. The excitation of the complexes was performed using a 375 nm laser diode (EPL-375, FWHM 100 ps). Emissions were collected until 10,000 counts were reached at the maximum emission of each compound. Emission lifetimes were determined from the emission decays using the deconvolution fit from F980 V1.4 software. The goodness-of-fit was assessed by examining residuals that were randomly distributed around zero and a chi-squared value between 0.9 and 1.2. Single crystal X-ray diffraction analysis (XRD) for **L2** (CCDC 2551507), **L3** (CCDC 2544725), and **C1** (CCDC 2544727), was performed with a STOE IPDS II two-circle diffractometer (Darmstadt, Germany) using Mo Kα radiation (λ = 0.71073 Å). The intensities were corrected for absorption using an empirical X-Area correction [34]. The structures were solved by direct methods (SHELXS) [35] and refined by full-matrix least-squares calculations on F2 (SHELXL-97). Absorbance measurements for cell viability assays in microplates

were performed using a Cytation 5 cell imaging multimode reader from Biotek (Winooski, VT, USA).

3.2. General Synthesis of N,N Ligands

Under a nitrogen atmosphere, a Buchwald–Hartwig amination was carried out by adding $Pd(dba)_2$ (0.03 equiv) and *rac*-BINAP (0.06 equiv) to a reaction flask containing dry toluene. The mixture was stirred until a color change was observed (ca. 30 min). Then, the corresponding amine (1.1 equiv) and halogenated compound (1.0 equiv) were added, and the mixture was stirred until complete dissolution, followed by the addition of potassium *tert*-butoxide (1.4 equiv). The reaction mixture was heated at reflux for 24 h. After completion of the reaction, the solvent was removed under reduced pressure, and the crude product was purified by column chromatography on silica gel using petroleum ether/ethyl acetate (30–50%) as the eluent. This procedure was used to obtain the intermediate ligands (**L1′**–**3′**) and, later, the final ligands (**L1**–**3**). For the spectroscopic details, see the Supplementary Materials.

Ligand L1. White powder, 55% yield (224 mg, 508.4 mmol). ^{1}H NMR (400 MHz, $CDCl_3$, 298 K): δ/ppm = 8.13 (d, *J* = 2.4 Hz, 1H), 8.04 (dt, *J* = 7.7, 1.0 Hz, 2H), 7.43–7.38 (m, 4H), 7.36–7.29 (m, 4H), 7.26–7.21 (m, 2H), 7.18 (tc, *J* = 7.53 Hz, 2H), 6.90 (d, *J* = 8.4 Hz, 2H), 2.20 (s, 6H).^{13}C{^{1}H} RMN (100 MHz, $CDCl_3$, 298 K): δ/ppm = 156.17, 148.90, 144.45, 140.89, 138.75, 133.57, 128.11, 127.85, 126.72, 125.93, 123.34, 120.31, 119.91, 117.28, 110.05, 17.91. FT-IR (ATR): ν/cm^{-1} = 1598, 1509, 1469, 1450, 1380, 1313, 1272, 1228, 1024, 826, 749, 724, 627, 574, 516, 418. Elemental analysis ($C_{30}H_{24}N_4$): calc: C 81.79; H 5.49; N 12.72. Found: C 80.96; H 5.58; N 12.61.

Ligand L2. White powder, 63% yield (446 mg, 943.8 mmol). ^{1}H RMN (400 MHz, $CDCl_3$, 298 K): δ/ppm = 7.98–7.94 (m, 4H), 7.36–7.28 (m, 4H), 7.24 (ddd, *J* = 8.2, 7.0, 1.2 Hz, 2H), 7.14–7.07 (m, 4H), 7.02 (dd, *J* = 8.9, 3.1 Hz, 2H), 6.85 (d, *J* = 8.9 Hz, 2H), 3.64 (s, 6H).^{13}C{^{1}H} RMN (100 MHz, $CDCl_3$, 298 K): δ/ppm = 152.14, 151.79, 144.73, 140.76, 134.90, 132.63, 127.61, 125.78, 125.25, 123.93, 123.11, 120.13, 119.72, 118.35, 109.86, 55.81. FT-IR (ATR): ν/cm^{-1} = 1571, 1450, 1389, 1314, 1262, 1229, 1180, 1031, 1010, 827, 751, 725, 627, 578, 532, 444, 419. Elemental analysis ($C_{30}H_{24}N_4O_2$): calc: C 76.25; H 5.12; N 11.86. Found: C 74.63; H 5.28; N 11.49.

Ligand L3. White powder, 88% yield (386 mg, 703.7 mmol). ^{1}H RMN (400 MHz, $CDCl_3$, 298 K): δ/ppm = 8.51 (s, 2H), 8.02 (d, *J* = 7.6 Hz, 2H), 7.73 (dd, *J* = 8.8, 2.7 Hz, 2H), 7.52 (d, *J* = 8.2 Hz, 2H), 7.40 (d, *J* = 8.2 Hz, 2H), 7.36–7.24 (m, 4H), 7.18 (t, *J* = 7.4 Hz, 2H), 7.12 (d, *J* = 8.6 Hz).^{13}C{^{1}H} RMN (100 MHz, $CDCl_3$, 298 K): δ/ppm = 159.50, 145.95, 142.93, 140.57, 136.66, 135.09, 129.53, 128.50, 126.16, 123.80 (q, J^{C-F}= 271.1 Hz), 123.64, 121.56 (q, J^{C-F}= 33.3 Hz), 120.51, 120.40, 116.33, 109.86. ^{19}F RMN (400 MHz, $CDCl_3$, 298 K): δ/ppm = −61.85. FT-IR (ATR): ν/cm^{-1} = 2927, 1595, 1514, 1481, 1453, 1395, 1312, 269, 1231, 1164, 1108, 1078, 1009, 940, 834, 750, 724, 676, 647, 618, 603, 540, 524, 512, 425. Elemental analysis ($C_{30}H_{18}F_6N_4$): calc: C 65.59; H 3.31; N 10.21. Found: C 67.02; H 3.22; N 9.96.

3.3. General Synthesis of Heteroleptic Cu(I) Complexes

In a sealed, nitrogen-purged vial, one equivalent of $[Cu(CH_3CN)_4]PF_6$, one equivalent of ligand (**L1**–**3**), and one equivalent of diphenylphosphino-phenyl ether were dissolved in anhydrous dichloromethane. The resulting solution was stirred at room temperature for 30 min. Then, the reaction mixture was filtered, and the filtrate was concentrated under reduced pressure. The crude product was recrystallized from a mixture of dichloromethane and toluene at a low temperature (−20 °C).

Complex C1. White crystalline solid, 97% yield (261 mg, 220.2 mmol). ^{1}H NMR (400 MHz, $CDCl_3$, 298 K): δ/ppm = 8.14 (d, *J* = 7.6 Hz, 2H), 7.77–7.70 (m, 2H), 7.56 (dd,

J = 8.5, 2.4 Hz, 2H), 7.49 (d, *J* = 8.3 Hz, 2H), 7.44–7.39 (m, 2H), 7.38–7.27 (m, 10H), 7.26–7.19 (m, 10H), 7.16 (d, *J* = 8.4 Hz, 2H), 7.12–7.01 (m, 12H), 6.90–6.83 (m, 2H), 1.85 (s, 6H).$^{13}C\{^1H\}$ RMN (100 MHz, $CDCl_3$, 298 K): δ/ppm = 157.85, 153.15, 149.31, 142.61, 140.94, 140.70, 135.01, 134.34, 133.28 (t, J^{C-P} = 8.2 Hz), 132.23, 130.92 (t, J^{C-P} = 10.3 Hz), 130.86, 130.70, 130.33, 128.98, 128.77, 126.15, 125.34, 124.76, 124.33 (t, J^{C-P} = 13.9 Hz), 123.49, 120.52, 120.35, 120.32, 120.24, 109.83, 17.50. ^{19}F RMN (400 MHz, $CDCl_3$, 298 K): δ/ppm = −74.09 (d, J^{F-P} = 720.5 Hz). $^{31}P\{^1H\}$ NMR (160 MHz, $CDCl_3$, 298 K): δ/ppm = −13.29 (s), −144.62 (hept, J^{P-F} = 717.0 Hz). FT-IR (ATR): ν/cm^{-1} = 1434, 1220, 837, 746, 694, 556, 509, 419. Elemental analysis ($C_{66}H_{52}CuF_6N_4OP_3$): calc: C 66.75; H 4.41; N 4.72. Found: C 68.12; H 4.69; N 4.58.

Complex C2. White crystalline solid, 94% yield (243 mg, 198.9 mmol). ^1H NMR (400 MHz, $CDCl_3$, 298 K): δ/ppm = 8.11 (d, *J* = 7.7 Hz, 2H), 7.69–7.64 (m, 4H), 7.51 (dd, *J* = 9.0, 3.0 Hz, 2H), 7.35–7.29 (m, 6H), 7.29–7.23 (m, 4H), 7.22–7.15 (m, 10H), 7.08–6.99 (m, 12H), 6.95 (dt, *J* = 8.2, 2.7 Hz, 2H), 6.88–6.82 (m, 2H), 6.82–6.76 (m, 2H), 3.41 (s, 6H).$^{13}C\{^1H\}$ RMN (100 MHz, $CDCl_3$, 298 K): δ/ppm = 157.55 (t, J^{C-P} = 6.0 Hz), 154.88, 147.06, 144.69, 140.97, 136.40, 134.04, 133.33 (t, J^{C-P} = 8.1 Hz), 132.21, 131.44, 130.54 (t, J^{C-P} = 16.7 Hz), 130.33, 128.95 (t, J^{C-P} = 4.8 Hz), 128.35, 126.33, 125.88, 125.52, 125.35, 124.54 (t, J^{C-P} = 14.0 Hz), 123.08, 120.44, 120.20, 119.78, 117.90, 109.76, 55.91. ^{19}F RMN (400 MHz, $CDCl_3$, 298 K): δ/ppm = −73.99 (d, J^{F-P} = 721.4 Hz) $^{31}P\{^1H\}$ NMR (160 MHz, $CDCl_3$, 298 K): δ/ppm = −13.29 (s), −144.66 (hept, J^{P-F} = 712.6 Hz). FT-IR (ATR): ν/cm^{-1} = 1571, 1491, 1469, 1451, 1437, 1389, 1326, 1263, 1231, 1180, 1031, 828, 751, 726, 693, 627, 578, 556, 509, 444, 420. Elemental analysis ($C_{66}H_{52}CuF_6N_4O_3P_3$): calc: C 65.00; H 4.30; N 4.59. Found: C 64.18; H 4.37; N 4.52.

Complex C3. Light-yellow crystalline solid, 93% yield (220 mg, 169.6 mmol). ^1H NMR (400 MHz, $CDCl_3$, 298 K): δ/ppm = 8.22 (s, 2H), 8.12 (d, *J* = 7.8 Hz, 2H), 7.85 (d, *J* = 8.3 Hz, 2H), 7.72 (dd, *J* = 9.1, 2.5 Hz, 2H), 7.60 (dd, *J* = 11.2, 8.3 Hz, 4H), 7.47 (t, *J* = 7.7 Hz, 2H), 7.39 (q, *J* = 7.5 Hz, 6H), 7.29 (td, *J* = 7.6, 2.6 Hz, 10H), 7.16–7.03 (m, 12H), 6.98 (d, *J* = 9.0 Hz, 2H), 6.91–6.84 (m, 2H).$^{13}C\{^1H\}$ RMN (100 MHz, $CDCl_3$, 298 K): δ/ppm = 158.46, 157.88 (t, J^{C-P} = 5.9 Hz), 145.59, 140.25, 139.57, 139.22, 136.68, 134.75, 132.98 (t, J^{C-P} = 8.0 Hz), 132.62, 131.34, 130.73, 130.07 (t, J^{C-P} = 17.2 Hz), 129.71, 129.28 (t, J^{C-P} = 4.8 Hz), 126.52, 125.69, 123.91, 123.19 (t, J^{C-P} = 15.1 Hz), 121.88 (q, J^{C-F}= 34.3 Hz), 120.78, 120.39, 120.44, 117.84, 110.03. ^{19}F RMN (400 MHz, $CDCl_3$, 298 K): δ/ppm = −62.55, −73.29 (d, J^{F-P} = 712.8 Hz). $^{31}P\{^1H\}$ RMN (160 MHz, $CDCl_3$, 298 K): δ/ppm = −13.50, −144.34 (hept, J^{P-F} = 712.9 Hz). FT-IR (ATR): ν/cm^{-1} = 1609, 1509, 1451, 1435, 1395, 1311, 1128, 1084, 1019, 913, 829, 745, 724, 693, 626, 555, 510, 451, 419. Elemental analysis ($C_{66}H_{46}CuF_{12}N_4OP_3$): calc: C 61.19; H 3.58; N 4.32. Found: C 62.84; H 3.47; N 4.19.

3.4. Cell Viability Assay

Human melanoma A375 cells were obtained from Sigma-Aldrich (ECACC, catalog number 88113005). This cell line is reported to harbor the BRAF V600E mutation, a key oncogenic driver in melanoma [36]. Cells were cultured in DMEM high-glucose medium supplemented with 10% fetal bovine serum (FBS) and maintained at 37 °C in a humidified 5% CO_2 atmosphere. Cells were seeded in 96-well plates at a density of 5000 cells per well and allowed to adhere for 24 h prior to exposure to serial dilutions (0.005–50 μM) of the tested compounds under both dark and light conditions. Stock solutions were prepared in DMSO and further diluted in culture medium, ensuring a final DMSO concentration of ≤0.5%, which showed no detectable cytotoxic effect under the experimental conditions. Cisplatin was dissolved in DMF to prepare a stock solution for use in the biological assay.

For dark experiments, cells were seeded in 96-well plates and incubated with the compounds for 48 h prior to adding the Neutral Red reagent. For light experiments,

cells were incubated with the compounds for 2 h in phenol red-free DMEM, followed by photoirradiation for 10 min using a photoirradiation box equipped with a 390 nm Kessil LED (see Figure S42), and further incubated to complete a total exposure time of 48 h from the initial compound addition.

Subsequently, the accumulated dye was extracted, and absorbance was measured at 540 nm to determine cell viability using a microplate reader (Cytation 5, Biotek). Dose–response curves were generated using GraphPad Prism V10.3.1 software. Each experiment was performed in triplicate within each run, and three independent experiments were conducted to assess reproducibility and calculate error estimates.

4. Conclusions

A series of three new heteroleptic Cu(I) complexes featuring functionalized dipyridylamine ligands and DPEphos was successfully synthesized in high yields and fully characterized. Structural analysis, including single-crystal X-ray diffraction of **C1**, confirms a mononuclear distorted tetrahedral geometry around the Cu(I) center, with the dpa ligand forming a six-membered metallacycle that adopts a boat-like conformation.

Absorption and emission studies show that all complexes have similar absorption profiles, mainly due to ligand-centered and MLCT transitions. However, their emission properties vary greatly depending on the electronic nature of the substituents. Notably, the CF_3-substituted complex demonstrates a significant red shift, which aligns with the stabilization of ligand-centered π^* orbitals. The emission is mostly unaffected by oxygen, indicating the involvement of short-lived excited states primarily of ^{1}MLCT character.

Biological evaluation shows that all complexes have significant cytotoxic activity in the low-micromolar range. Notably, only the CF_3-containing complex demonstrates a light-induced increase in cytotoxicity, highlighting its photoactivatable nature. This behavior indicates a direct link between excited-state electronic structure and the photobiological response, emphasizing the important role of ligand electronic effects in influencing both photophysical and biological properties. Further studies to elucidate the underlying mechanisms and improve photoresponse are currently underway.

Supplementary Materials: The following supporting information can be downloaded at: https://www.mdpi.com/article/10.3390/inorganics14050140/s1, (Figures S1–S46 and Tables S1 and S2).

Author Contributions: Conceptualization, A.V.-M. and A.R.C.; methodology, A.V.-M. and A.R.C.; validation, A.V.-M., M.A.F. and A.R.C.; formal analysis, A.V.-M. and I.B.; investigation, A.V.-M., M.H.-M., I.B., M.P., S.M.-F. and A.R.C.; resources, A.V.-M., I.B., M.A.F. and A.R.C.; writing—original draft preparation, A.V.-M. and A.R.C.; writing—review and editing, A.V.-M. and A.R.C.; visualization, A.V.-M. and A.R.C.; supervision, A.R.C.; project administration, A.V.-M. and A.R.C.; funding acquisition, A.V.-M. and A.R.C. All authors have read and agreed to the published version of the manuscript.

Funding: This research was funded by ANID Fondecyt Postdoctoral fellowship 3230413. Fondequip program EQM 160042, EQM 120021, EQM 130021, EQM 180024. 39175004-301-81 "Apoyo Investigación Básica Química 2025" DIPOG-UC. 39171019-301-81 Proyecto Puente 2025 VRI-UC.

Institutional Review Board Statement: Not applicable.

Informed Consent Statement: Not applicable.

Data Availability Statement: Data are contained within the article and supplementary materials.

Acknowledgments: We gratefully acknowledge Denis Fuentealba and Rodrigo Montecinos (Facultad de Química y de Farmacia, Pontificia Universidad Católica de Chile) for providing access to the emission instrumentation. We also thank Claudio López (Facultad de Química y de Farmacia, Pontificia Universidad Católica de Chile) for his valuable assistance in the design and 3D printing of the photoirradiation box.

Conflicts of Interest: The authors declare no conflicts of interest.

References

1. Beaudelot, J.; Oger, S.; Perusko, S.; Phan, T.A.; Teunens, T.; Moucheron, C.; Evano, G. Photoactive Copper Complexes: Properties and Applications. *Chem. Rev.* **2022**, *122*, 16365–16609. [CrossRef]
2. Forster, C.; Heinze, K. Photophysics and photochemistry with Earth-abundant metals—Fundamentals and concepts. *Chem. Soc. Rev.* **2020**, *49*, 1057–1070. [CrossRef] [PubMed]
3. Naina, V.R.; Singh, A.K.; Krätschmer, F.; Lebedkin, S.; Kappes, M.M.; Roesky, P.W. Heteroleptic copper(I) complexes with coumarin-substituted aminodiphosphine and diimine ligands: Synthesis and photophysical studies. *Dalton Trans.* **2023**, *52*, 12618–12622. [CrossRef]
4. Appleby, M.V.; Cowin, R.A.; Ivalo, I.I.; Peralta-Arriaga, S.L.; Robertson, C.C.; Bartlett, S.; Fitzpatrick, A.; Dent, A.; Karras, G.; Diaz-Moreno, S.; et al. Ultrafast electronic, infrared, and X-ray absorption spectroscopy study of Cu(i) phosphine diimine complexes. *Faraday Discuss.* **2023**, *244*, 391–410. [CrossRef]
5. Iwamura, M.; Takeuchi, S.; Tahara, T. Ultrafast Excited-State Dynamics of Copper(I) Complexes. *Acc. Chem. Res.* **2015**, *48*, 782–791. [CrossRef]
6. Sosoe, J.; Cruché, C.; Morin, M.; Collins, S.K. Evaluating heteroleptic copper(I)-based complexes bearing π-extended diimines in different photocatalytic processes. *Can. J. Chem.* **2020**, *98*, 461–465. [CrossRef]
7. Takeda, H.; Monma, Y.; Ishitani, O. Highly Functional Dinuclear Cu(I)-Complex Photosensitizers for Photocatalytic CO_2 Reduction. *ACS Catal.* **2021**, *11*, 11973–11984. [CrossRef]
8. Wang, Y.Q.; Tang, T.X.; Yuan, Y.; Li, N.; Wang, X.Q.; Guan, J. Copper and Copper Complexes in Tumor Therapy. *ChemMedChem* **2024**, *19*, e202400060. [CrossRef] [PubMed]
9. Marion, R.; Sguerra, F.; Di Meo, F.; Sauvageot, E.; Lohier, J.F.; Daniellou, R.; Renaud, J.L.; Linares, M.; Hamel, M.; Gaillard, S. NHC Copper(I) Complexes Bearing Dipyridylamine Ligands: Synthesis, Structural, and Photoluminescent Studies. *Inorg. Chem.* **2014**, *53*, 9181–9191. [CrossRef] [PubMed]
10. Villegas-Menares, A.; Hansmann, Y.B.; Bayas, M.; Verdugo, C.; Erazo, I.; Zuñiga, C.; Gonzalez, I.; Galdámez, A.; Villa, L.; Natali, M.; et al. Exploring catalytic activity modulations: Photoredox catalysis with substituted copper(I)-dipyridylamine derivatives. *Dalton Trans.* **2025**, *54*, 7306–7314. [CrossRef]
11. Wang, S.; Bruneau, C.; Renaud, J.L.; Gaillard, S.; Fischmeister, C. 2,2′-Dipyridylamines: More than just sister members of the bipyridine family. Applications and achievements in homogeneous catalysis and photoluminescent materials. *Dalton Trans.* **2019**, *48*, 11599–11622. [CrossRef]
12. Giobbio, G.; Montrieul, A.; Lohier, J.F.; Costa, R.D.; Gaillard, S. Economic and Straightforward Synthesis of Heteroleptic Silver(I) Complexes bearing NHC and Bidentate Ligands. *Eur. J. Inorg. Chem.* **2025**, *28*, e202500030. [CrossRef]
13. Elie, M.; Sguerra, F.; Di Meo, F.; Weber, M.D.; Marion, R.; Grimault, A.; Lohier, J.F.; Stallivieri, A.; Brosseau, A.; Pansu, R.B.; et al. Designing NHC-Copper(I) Dipyridylamine Complexes for Blue Light-Emitting Electrochemical Cells. *ACS Appl. Mater. Inter.* **2016**, *8*, 14678–14691. [CrossRef]
14. Elie, M.; Mahoro, G.U.; Duverger, E.; Renaud, J.L.; Daniellou, R.; Gaillard, S. Cytotoxicity of cationic NHC copper(I) complexes coordinated to 2,2′-bis-pyridyl ligands. *J. Organomet. Chem.* **2019**, *893*, 21–31. [CrossRef]
15. Abdolmaleki, S.; Aliabadi, A.; Khaksar, S. Unveiling the promising anticancer effect of copper-based compounds: A comprehensive review. *J. Cancer Res. Clin. Oncol.* **2024**, *150*, 213. [CrossRef]
16. Ceramella, J.; Mariconda, A.; Iacopetta, D.; Saturnino, C.; Barbarossa, A.; Caruso, A.; Rosano, C.; Sinicropi, M.S.; Longo, P. From coins to cancer therapy: Gold, silver and copper complexes targeting human topoisomerases. *Bioorg. Med. Chem. Lett.* **2020**, *30*, 126905. [CrossRef]
17. Molinaro, C.; Martoriati, A.; Pelinski, L.; Cailliau, K. Copper Complexes as Anticancer Agents Targeting Topoisomerases I and II. *Cancers* **2020**, *12*, 2863. [CrossRef] [PubMed]
18. Khan, R.A.; Usman, M.; Dhivya, R.; Balaji, P.; Alsalme, A.; AlLohedan, H.; Arjmand, F.; AlFarhan, K.; Akbarsha, M.A.; Marchetti, F.; et al. Heteroleptic Copper(I) Complexes of "Scorpionate" Bis-pyrazolyl Carboxylate Ligand with Auxiliary Phosphine as Potential Anticancer Agents: An Insight into Cytotoxic Mode. *Sci. Rep.* **2017**, *7*, 45229. [CrossRef]
19. Thomas, A.; Pommier, Y. Targeting Topoisomerase I in the Era of Precision Medicine. *Clin. Cancer Res.* **2019**, *25*, 6581–6589. [CrossRef]
20. Gourdon, L.; Cariou, K.; Gasser, G. Phototherapeutic anticancer strategies with first-row transition metal complexes: A critical review. *Chem. Soc. Rev.* **2022**, *51*, 1167–1195. [CrossRef] [PubMed]
21. Al Hageh, C.; Al Assaad, M.; El Masri, Z.; Samaan, N.; El-Sibai, M.; Khalil, C.; Khnayzer, R.S. A long-lived cuprous bis-phenanthroline complex for the photodynamic therapy of cancer. *Dalton Trans.* **2018**, *47*, 4959–4967. [CrossRef]
22. Lin, R.K.; Chiu, C.I.; Hsu, C.H.; Lai, Y.J.; Venkatesan, P.; Huang, P.H.; Lai, P.S.; Lin, C.C. Photocytotoxic Copper(II) Complexes with Schiff-Base Scaffolds for Photodynamic Therapy. *Chem. Eur. J.* **2018**, *24*, 4111–4120. [CrossRef]

23. Smith, C.B.; Days, L.C.; Alajroush, D.R.; Faye, K.; Khodour, Y.; Beebe, S.J.; Holder, A.A. Photodynamic Therapy of Inorganic Complexes for the Treatment of Cancer. *Photochem. Photobiol.* **2022**, *98*, 17–41. [CrossRef]
24. Wahengbam, S.; Musib, D.; Roy, M. Recent Advances on the Development of Early Transition Metal Complexes for Photo-Assisted Cytotoxicity Applications. *Chemistryselect* **2024**, *9*, e202302969. [CrossRef]
25. Imberti, C.; Zhang, P.Y.; Huang, H.Y.; Sadler, P.J. New Designs for Phototherapeutic Transition Metal Complexes. *Angew. Chem. Int. Ed.* **2020**, *59*, 61–73. [CrossRef]
26. Gaillard, S.; Elmkaddem, M.K.; Fischmeister, C.; Thomas, C.M.; Renaud, J.L. Highly efficient and economic synthesis of new substituted amino-bispyridyl derivatives via copper and palladium catalysis. *Tetrahedron Lett.* **2008**, *49*, 3471–3474. [CrossRef]
27. Okuniewski, A.; Rosiak, D.; Chojnacki, J.; Becker, B. Coordination polymers and molecular structures among complexes of mercury(II) halides with selected 1-benzoylthioureas. *Polyhedron* **2015**, *90*, 47–57. [CrossRef]
28. Henriquez, M.A.; Engl, S.; Jaque, P.; Gonzalez, I.A.; Natali, M.; Reiser, O.; Cabrera, A.R. Phosphine Evaluation on a New Series of Heteroleptic Copper(I) Photocatalysts with dpa Ligand [Cu(dpa)(P,P)]BF4. *Eur. J. Inorg. Chem.* **2021**, *2021*, 4020–4029. [CrossRef]
29. Cuttell, D.G.; Kuang, S.M.; Fanwick, P.E.; McMillin, D.R.; Walton, R.A. Simple Cu(I) complexes with unprecedented excited-state lifetimes. *J. Am. Chem. Soc.* **2002**, *124*, 6–7. [CrossRef]
30. Levitus, M. Tutorial: Measurement of fluorescence spectra and determination of relative fluorescence quantum yields of transparent samples. *Method. Appl. Fluoresc.* **2020**, *8*, 033001. [CrossRef]
31. Housecroft, C.E.; Constable, E.C. TADF: Enabling luminescent copper(I) coordination compounds for light-emitting electrochemical cells. *J. Mater. Chem. C* **2022**, *10*, 4456–4482. [CrossRef] [PubMed]
32. Czerwieniec, R.; Leitl, M.J.; Homeier, H.H.H.; Yersin, H. Cu(I) complexes—Thermally activated delayed fluorescence. Photophysical approach and material design. *Coord. Chem. Rev.* **2016**, *325*, 2–28. [CrossRef]
33. Tao, S.; Liu, N.; Dai, B. One-pot two-step synthesis of N-arylcarbazole-based skeleton. *RSC Adv.* **2016**, *6*, 43250–43260. [CrossRef]
34. STOE; Cie GmbH. *X-STEP32, Version 1.07 b: Crystallographic Package*; STOE & Cie GmbH: Darmstadt, Germany, 2000.
35. Sheldrick, G.M. SHELXT—Integrated space-group and crystal-structure determination. *Acta Cryst.* **2015**, *71*, 3–8. [CrossRef] [PubMed]
36. Al Hashmi, M.; Konduru, S.S.; Silcock, L.; Chouchane, L.; Mattei, V.; James, N.; Mathew, R.; Bedognetti, D.; De Giorgi, V.; Murtas, D.; et al. Differential responsiveness to BRAF inhibitors of melanoma cell lines BRAF V600E-mutated. *J. Transl. Med.* **2020**, *18*, 192. [CrossRef]

Disclaimer/Publisher's Note: The statements, opinions and data contained in all publications are solely those of the individual author(s) and contributor(s) and not of MDPI and/or the editor(s). MDPI and/or the editor(s) disclaim responsibility for any injury to people or property resulting from any ideas, methods, instructions or products referred to in the content.